

Effect of Weak Rotation on Large-Scale Circulation Cessations in Turbulent Convection

Michael Assaf,¹ Luiza Angheluta,^{1,2} and Nigel Goldenfeld¹

¹*Department of Physics, University of Illinois at Urbana-Champaign, Loomis Laboratory of Physics, 1110 West Green Street, Urbana, Illinois 61801-3080, USA*

²*Physics of Geological Processes, Department of Physics, University of Oslo, Norway*
(Received 13 May 2012; published 16 August 2012)

We investigate the effect of weak rotation on the large-scale circulation (LSC) of turbulent Rayleigh-Bénard convection, using the theory for cessations in a low-dimensional stochastic model of the flow previously studied. We determine the cessation frequency of the LSC as a function of rotation, and calculate the statistics of the amplitude and azimuthal velocity fluctuations of the LSC as a function of the rotation rate for different Rayleigh numbers. Furthermore, we show that the tails of the reorientation PDF remain unchanged for rotating systems, while the distribution of the LSC amplitude and correspondingly the cessation frequency are strongly affected by rotation. Our results are in close agreement with experimental observations.

DOI: [10.1103/PhysRevLett.109.074502](https://doi.org/10.1103/PhysRevLett.109.074502)

PACS numbers: 47.27.te, 05.65.+b, 47.27.eb

The complex phenomenon of thermal turbulence, also known as turbulent Rayleigh-Bénard convection, develops in a heated fluid layer under gravity by a succession of instabilities in the thermal transport due to an interplay between different driving forces such as buoyancy, viscous drag, and diffusion. This balance between different transport mechanisms is quantified by the Rayleigh number $Ra = \alpha_0 g \Delta T L^3 / \nu \kappa$ determining the flow state. Here, α_0 is the isobaric thermal expansion coefficient, g is the acceleration of gravity, ΔT is the temperature gap between the bottom and top plates, L is the height of the fluid container, κ is the thermal diffusivity, and ν is the kinematic viscosity. When Ra is sufficiently large, the flow becomes turbulent and a large-scale circulation (LSC) is formed. The latter is maintained by the emission of plumes from the top and bottom surfaces which, due to buoyancy, move upwards (hot plumes) or downwards (cold plumes) [1–3]. This LSC is known to appear in various *rotating* natural systems, such as atmospheric [4] and oceanic flows [5], and the dynamo driving planetary magnetic fields [6].

Such a circulating state does not persist indefinitely, however, and cessations followed by restarted flows at a new azimuthal angle occur sporadically [3,7–10]. The complex dynamics of the LSC is influenced by the heat and momentum transport mechanisms, as well as by the geometry and aspect ratio Γ (diameter over height) of the fluid container. In experiments using a cylindrical geometry with $\Gamma = 1$, the LSC occurs in a nearly vertical plane, whereas for the aspect ratio $\Gamma = 0.5$, two convection rolls may coexist [11]. Recent studies also report that the LSC flow reversals and its tilted orientation are strongly influenced by the corner flows that form in a rectangular geometry [12]. The dynamics of a nearly vertical, single LSC can be modeled by a set of nonlinear stochastic differential equations that describe the amplitude of azimuthal temperature variations, δ , and the azimuthal orientation angle,

θ_0 [13,14]. This model is found to be in excellent agreement with the typical fluctuations of the LSC [13,14]. Yet, the cessations require an extension of the model since boundary terms describing the thermal and viscous diffusion become dominant terms when the amplitudes are small, as they inevitably must be during a cessation. With this extension, the model is able to provide an excellent description of the cessation rates, as well as the LSC amplitude and azimuthal velocity probability distribution functions (PDFs) including the tails [15].

The purpose of this Letter is to study the effect of weak rotation on the statistics of the main degrees of freedom, i.e., amplitude and azimuthal velocity, and the LSC cessation events in Rayleigh-Bénard convection. Here the rotation rate Ω is conveniently represented by the dimensionless convective Rossby number, $Ro = (2\Omega)^{-1} \sqrt{\alpha_0 g \Delta T / L}$, which measures the buoyancy relative to the Coriolis force. The total heat transport, measured by the Nusselt number, \mathcal{N} , relative to heat diffusion, has a nontrivial dependence on Ro , exhibiting three different regimes [10,16,17]: (i) an LSC-dominant regime at $Ro^{-1} \leq Ro_c^{-1} \simeq 0.4$ where buoyancy dominates over Coriolis effects; (ii) an Ekman-vortex pumping regime at $Ro_c^{-1} < Ro^{-1} < Ro_{\max}^{-1}$ where the Coriolis force dominates over the buoyancy force for a nonvanishing Ro_c^{-1} ; and (iii) a regime at $Ro^{-1} > Ro_{\max}^{-1}$ (typically $Ro_{\max}^{-1} \simeq 3 - 10$ depending on Ra [10]) where the velocity gradients, and thus heat transport by convection, are suppressed via the Taylor-Proudman effect [10]. Here Ro_c^{-1} scales as $1/\Gamma$ due to a finite-size effect [18,19], while Ro_{\max}^{-1} is determined by an interplay between the Ekman enhancement and the Taylor-Proudman depression.

In this work we focus only on weak rotations, where the LSC is still present, namely in the regime $0 < Ro^{-1} \leq 0.6$. Recent experimental studies report a nonmonotonic dependence of the LSC mean amplitude on $\Omega \sim Ro^{-1}$ [10]. The

mean amplitude initially increases with increasing Ro^{-1} until Ro^{-1} becomes close to (but below) a critical value, Ro_c^{-1} . The origin of this increase is not well understood, but may be associated with centripetal effects [20]; see below. For higher Ro^{-1} , the detaching plumes from the thermal boundary layers (BLs) interact with the Ekman-vortex structure that forms at Ro_c^{-1} , so that these plumes can no longer feed the LSC [21]. Thus, the mean amplitude decreases at $Ro^{-1} \gtrsim Ro_c^{-1}$. For $Ro^{-1} \gtrsim 0.6 - 1$ (depending on Ra, Prandtl number, and Γ), the mean amplitude becomes comparable to the root-mean-square temperature fluctuations about the mean, and thus becomes ill defined [10]. This nonmonotonic behavior of the LSC mean amplitude on Ro^{-1} is accompanied by a nonmonotonic behavior of the LSC cessation frequency, and this is what we calculate below. This dependence contrasts with our result for the tails of the reorientation statistics, namely the probability for a large angle change in the LSC plane, which we show is almost independent of the rotation strength in this weak rotation regime.

Statistics of the LSC dynamics with rotation.—The evolution of the dimensionless LSC amplitude, ξ , and azimuthal angle, θ_0 , in the absence of rotations is governed by the stochastic differential equations [15]

$$\begin{aligned} \dot{\xi} &= A + \alpha\xi - \beta\xi^{3/2} + f_\xi(t), \\ \dot{\theta}_0 &= -\left(\alpha_1\xi + \beta_1\frac{\tau_\theta}{\tau_\delta}\sqrt{\xi}\right)\dot{\theta}_0 + f_\theta(t). \end{aligned} \quad (1)$$

Here, A is a constant related to the heat transport or the inverse of the thermal BL width, $\xi = \delta/\delta_0$ is the dimensionless LSC amplitude, where δ is the physical LSC amplitude, $\delta_0 \approx \Delta T \sigma Re^{3/2}/Ra$ is the mean LSC amplitude, and $\sigma = \nu/\kappa$ is the Prandtl number. Furthermore, the Reynolds number is defined as $Re = (\tau_\delta/\tau_\theta)^2 \gg 1$, where τ_δ and τ_θ are the turnover times in the LSC and azimuthal planes, respectively, while time in Eq. (1) is measured in units of the corresponding turnover times τ_δ and τ_θ [15]. Also, delta-correlated Gaussian stochastic forcing terms $f_\delta(t)$ and $f_\theta(t)$ with amplitudes D_δ and D_θ are included in Eq. (1) to simulate the effect of turbulent fluctuations. Finally, the coefficients $\alpha, \beta, \alpha_1, \beta_1 = \mathcal{O}(1)$ are included to account for the geometric coefficients from the spatial volume averaging procedure [13,14]. Note, that in Eq. (1) all tildes (which appeared in Ref. [15] due to time rescaling) were removed for clarity.

In the presence of rotation, the equation for the LSC amplitude [the first of Eq. (1)] remains the same, since the same drag and buoyancy forces drive the motion of the LSC in the vertical plane. Yet, the coefficients in front of these terms may depend on Ro , to account for the experimental fact that the mean dimensionless LSC amplitude ξ_0 is a function of Ro^{-1} . To find this Ro dependence, we notice that the coefficients $\alpha(Ro)$, $\beta(Ro)$, and $A(Ro)$ are related to each other by the constraints that the PDF $P(\xi)$ is

centered around $\xi = \xi_0$ and has a width D_δ [15]. Employing these constraints, we obtain

$$\alpha(Ro) = 1 - 3A/\xi_0, \quad \beta(Ro) = \xi_0^{-1/2}(1 - 2A/\xi_0). \quad (2)$$

Now we formulate a simple theory that can explain the dependency of these coefficients as well as that of ξ_0 on Ω . We assume that $\alpha = \alpha_0$ is constant (because the geometrical coefficient in the buoyancy should not be affected by rotation) and expand $\beta = \beta_0(1 + b_1\Omega + b_2\Omega^2)$ (assuming that the thickness of the viscous BL is dependent on Ω), where $\alpha_0 = 1 - 3A_0$, $\beta_0 = 1 - 2A_0$, and $A_0 = A(\Omega = 0)$. In this way, we can find expressions for $A(\Omega)$ and $\xi_0(\Omega)$ by equating these expressions for α and β with Eq. (2), and keeping terms up to $\mathcal{O}(\Omega^2)$. We obtain $\xi_0(\Omega) \approx 1 - 2b_1\Omega + (3b_1^2 - 2b_2)\Omega^2$ and $A(\Omega) = A_0\xi_0(\Omega)$. Note that plugging this into Eq. (2), we obtain $\alpha(Ro) = \alpha_0$ and $\beta(Ro) \approx \beta_0\xi_0^{-1/2}$. Because $\beta(Ro)$ represents the inverse Rossby-dependent width of the viscous BL, the latter increases as $\xi_0^{1/2}$ for $0 < Ro^{-1} < Ro_c^{-1}$, in agreement with recent experimental observations [20,21]. The origin of the increase in the viscous BL width in the weak-rotation regime can be associated with centripetal effects [20] that tend to increase the BL width according to the Prandtl-Blasius theory.

In Fig. 1 we plot the experimental mean amplitude ξ_0 and A (normalized by their value at zero rotation) as a function of Ro^{-1} . According to our theory, provided that ξ_0 is well approximated by a parabolic expansion in Ω , in the weak rotation regime, A/A_0 should coincide with $\xi_0/\xi_0(0)$, and this is indeed the case. The insets in this figure confirm the dependencies of α and β on Ω for two different Ra numbers. Note that in order to extract A from the experimental data, we have used the relation $A = BD_\delta/2$ [15] where B and D_δ are specified below.

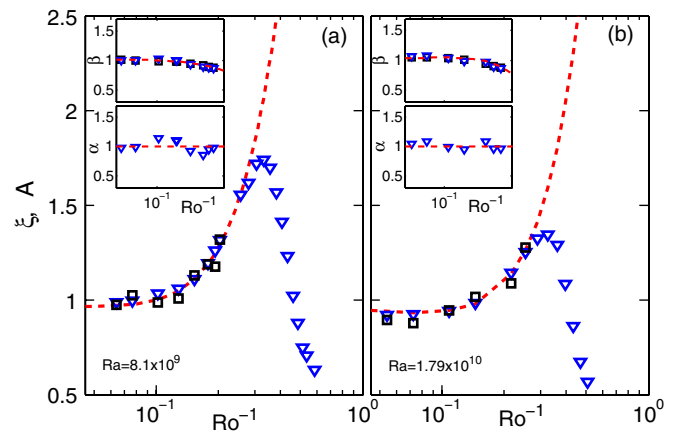


FIG. 1 (color online). Shown are the values of ξ_0 (triangles), and A (squares). The dashed line is a parabolic fit. The upper inset shows β (triangles) compared with $\xi_0^{-1/2}$ (squares), while the dashed line is a parabolic fit. The lower inset shows α and the dashed line is a guide for the eye. All quantities are normalized by their nonrotating values.

Since the equation for the LSC amplitude [the first of Eq. (1)] is independent of the azimuthal reorientation angle θ_0 , we can analyse it separately by writing the corresponding Fokker-Planck equation and finding its stationary solution [15]. Defining the potential

$$V(\xi) = -\frac{BD_\delta}{2}\xi - \left(1 - \frac{3BD_\delta}{2\xi_0}\right)\frac{\xi^2}{2} + \frac{2}{5\xi_0^{1/2}}\left(1 - \frac{BD_\delta}{\xi_0}\right)\xi^{5/2}, \quad (3)$$

the frequency-dependent PDF, $P(\xi, \text{Ro})$, takes the form

$$P(\xi, \text{Ro}) = Ce^{-2V(\xi)/D_\delta}. \quad (4)$$

Here C is a normalization constant, $D_\delta = D_\delta(\text{Ro})$ is the PDF width in the Gaussian regime, $P(\xi \approx \xi_0) \sim e^{-(\xi - \xi_0)^2/(2D_\delta)}$, and $B = B(\text{Ro})$ is the logarithmic derivative of the PDF at small ξ , since $P(\xi \ll 1) \sim e^{B\xi}$.

Furthermore, it has been shown that the cessation frequency—the frequency of events that the LSC amplitude goes below a threshold amplitude $\xi_{\min} \ll 1$ —is given by

$$\omega^{-1} = \frac{1}{\xi_{\min}} \int_0^{\xi_{\min}} d\xi^* T(\xi^*); \quad (5)$$

$$T(\xi^*) \sim e^{-2D^{-1}[V(\xi^*) - V(1)]}.$$

Here $T(\xi^*)$ is the mean time it takes the amplitude to reach $\xi^* \ll 1$.

In order to compare the results for the PDF [Eq. (4)] and cessation frequency [Eq. (5)] with experimental results, we extract the values of $B(\text{Ro})$ and $D_\delta(\text{Ro})$ from the experimental PDFs, just as was done for the nonrotating case [15]. In Fig. 2, we compare experimental and theoretical PDFs for different Ro and Ra numbers, in the weakly rotating regime. The theoretical predictions hold well for various rotation frequencies, provided that we use the corresponding frequency-dependent parameters. As $\text{Ro}^{-1} \sim \Omega$ is increased, the width of the PDF increases compared to the nonrotating case while the slope of the left tail decreases. This functional dependence of the experimental B and D_δ on Ro^{-1} is shown in the lower panels of Fig. 2 for two different Ra numbers.

Finally, in Fig. 3 we compare the theoretical and experimental results for the cessation frequency as functions of Ro for different Ra values and observe good agreement. Here, the threshold for cessation was chosen to be 0.15.

Rotation rate of the azimuthal plane:—In this section we investigate the effect of weak rotation on the PDF for the angular velocity of the azimuthal plane [the second of Eq. (1)]. Rotation brings about a Coriolis force which is proportional to $\vec{\Omega} \times \vec{V}_\theta$, where $|\vec{V}_\theta| \sim \xi$ [13]. As a result, the effect of rotation on the azimuthal dynamics amounts to the addition of a term of the form $\xi\Omega\Phi(\theta_0)$ to the equation for $\dot{\theta}_0$, where $\Phi = \mathcal{O}(1)$ is some function of the azimuthal angle [22]. Therefore, the second of Eq. (1) under rotation becomes

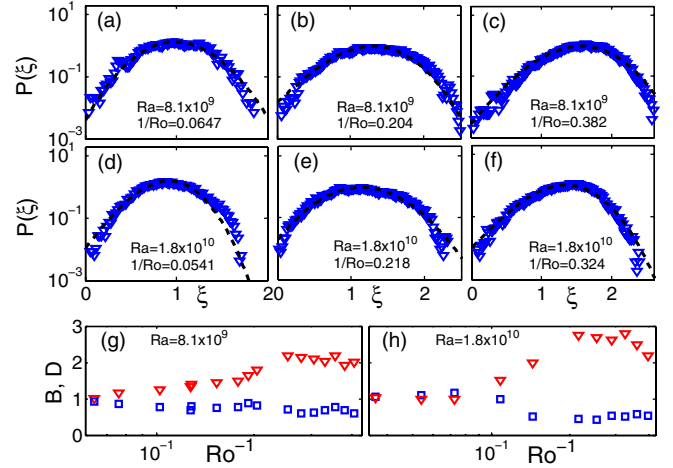


FIG. 2 (color online). Panels (a)–(f) show the PDFs of the LSC rescaled amplitude ξ for different Ro and Ra numbers. Each row represents a different Ra number. The experimental PDFs are represented by triangles, while the fitting curves (dashed line) are the analytical PDFs [Eq. (4)] with parameters B and D_δ determined experimentally for each Ro number. The width of the PDFs initially increases with increasing Ro^{-1} while the slope of the left tail decreases. This can be seen in panels (g) and (h) where we plot the experimental B (squares) and D_δ (triangles) as functions of Ro^{-1} for different Ra .

$$\ddot{\theta}_0 = \xi\Omega\Phi(\theta_0) - \left(\alpha_1\xi + \beta_1\frac{\tau_\theta}{\tau_\delta}\sqrt{\xi}\right)\dot{\theta}_0 + f_\theta(t). \quad (6)$$

As expected, the addition of the first term on the right-hand side of Eq. (6) changes the steady state solution for $\dot{\theta}$ at $\xi \approx 1$ from $\dot{\theta} = 0$ at zero rotation to $\dot{\theta} \sim \Omega$ at $\Omega > 0$ [since $\Phi(\theta_0) = \mathcal{O}(1)$ and $\tau_\theta/\tau_\delta \ll 1$]. This has been experimentally observed by Zhong and Ahlers [10] in the weakly rotating regime, below Ro_c^{-1} . The reason for this limitation is that the steady-state solution is valid only as long as the parameters involved are of order unity, which holds for not too large Ω , but breaks down for high rotation frequencies.

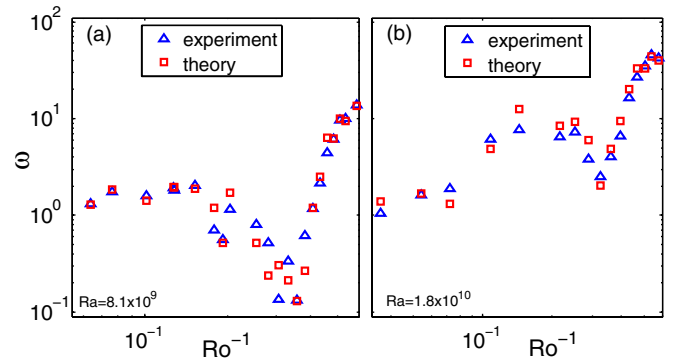


FIG. 3 (color online). Cessation frequency (normalized by its nonrotating value) as a function of Ro^{-1} for different values of Ra . The triangles are experimental results, while the squares are the theoretical predictions according to Eq. (5). The cessation threshold chosen here was 0.15.

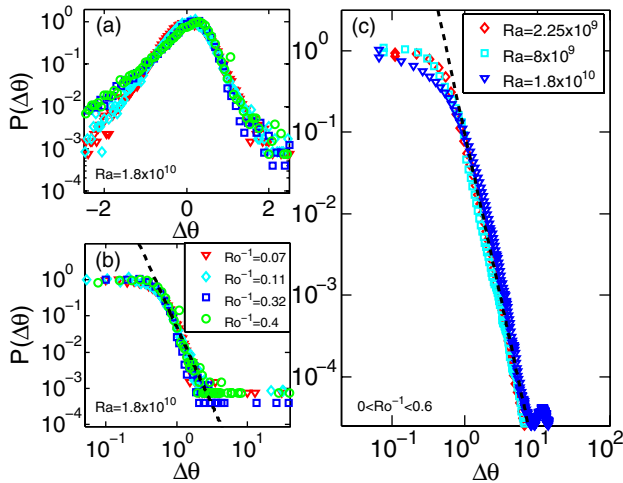


FIG. 4 (color online). PDF $P(\Delta\theta)$ as a function of $\Delta\theta$. Panel (a) shows the experimental PDFs for four different Ro numbers [see legend in panel (b)] for $Ra = 1.8 \times 10^{10}$. As $Ro^{-1} \sim \Omega$ increases, the left tail becomes fatter while the right tail remains more or less constant. Panel (b) shows the same PDFs on a log-log plot, demonstrating that the tail is well described by a power law independent of Ro ; the dashed line is a power law with exponent -4.3 . Panel (c) shows PDFs, averaged over a wide range of Ro^{-1} numbers (generally $0 < Ro^{-1} < 0.6$), for different Ra . The dashed line is the same as in panel (b). This panel implies that the rare-event statistics of $P(\Delta\theta)$ are universal and independent of Ra and Ro .

In the latter case, when Ekman vortices start to form, the model becomes invalid.

Apart from the steady-state solution that represents the mean angular velocity, here we are mainly interested in the rare events of large deviations in $\Delta\theta \sim \hat{\theta}$. The tails of the PDF $P(\Delta\theta)$ were calculated in Ref. [15] for nonrotating systems. Here, we show that these tails are unchanged by the rotation. The reason is that the term due to rotation added to Eq. (6) is proportional to ξ . As a result, large deviations in $\Delta\theta$, which occur when $\xi \ll 1$, are still governed by the term proportional to $\sqrt{\xi}\hat{\theta}_0$ in Eq. (6), which is dominant in the regime of $\xi \ll 1$ [15]. This term does not depend on the rotation frequency. Therefore, the tails of $P(\Delta\theta)$ remain unchanged when rotation is introduced, as shown in Fig. 4.

Indeed, in the nonrotating case the tails have been found to scale as a power law with exponent -4 , while experimental results for nonrotating systems demonstrate a power-law tail with exponent ~ -4.3 [15]. Figure 4(b) shows experimental PDFs, $P(\Delta\theta)$, for different Ro numbers. In panel (c) we show PDFs averaged over a wide range of Ro^{-1} numbers [10] (generally $0 < Ro^{-1} < 0.6$), for different Ra numbers. The dashed lines in panels (b) and (c) are the theoretical prediction: a power law curve with exponent -4.3 . The excellent agreement between theory and experiment indicates that the exponent for rotating systems remains unchanged compared to the

nonrotating case. Note that panels (b) and (c) are shown on a log-log scale which only allows us to show the positive $\hat{\theta}$ region. We have checked that the left and right tails of the PDF scale with the same exponent within 5%.

Angular-dependent asymmetry of the PDF for azimuthal fluctuations:—We conclude by pointing out an interesting corollary of our analysis. From Fig. 4(a), it is apparent that in contrast to the nonrotating case, the PDF $P(\Delta\theta)$ develops an asymmetric shape as a function of $\Delta\theta$ that is an increasing function of the rotation rate, up to the vicinity of $1/Ro \sim 1/Ro_c$. We speculate that this asymmetry in the azimuthal velocity fluctuations is related to spiral defects and their preferred motion. Near the onset of convection, spiral defects are formed in the presence of rotation and their azimuthal motion is *against* the direction of rotation [23]. With increasing Ra number, the flow becomes more turbulent and the effect of the individual vortices on the azimuthal velocity statistics diminishes [24]. However, as the strength of the LSC decreases when Ro^{-1} exceeds Ro_c^{-1} , the flow, hence the velocity statistics, is more influenced by the preferred motion of the spiral defects in the presence of rotation, which would explain the observed broadening of the left tail of the PDF $P(\Delta\theta)$ corresponding to high fluctuations against the direction of rotation. This effect of the left-tail broadening with increasing Ω can be clearly seen in Fig. 4(a). However, the mechanism relating the asymmetry in $P(\Delta\theta)$ to spiral defects needs further elaboration, and is beyond the scope of this Letter.

We thank J.-Q. Zhong and G. Ahlers for sharing with us their unpublished data on rotating Rayleigh-Bénard convection, shown in the figures. M. A. gratefully acknowledges the Center for the Physics of Living Cells at the University of Illinois for support. L. A. is grateful for support from the Center of Excellence for Physics of Geological Processes. This work was partially supported by the National Science Foundation through Grant No. NSF-DMR-1044901.

-
- [1] R. Krishnamurti and L. Howard, *Proc. Natl. Acad. Sci. U.S.A.* **78**, 1981 (1981).
 - [2] E. Siggia, *Annu. Rev. Fluid Mech.* **26**, 137 (1994).
 - [3] G. Ahlers, S. Grossmann, and D. Lohse, *Rev. Mod. Phys.* **81**, 503 (2009).
 - [4] E. van Doorn, B. Dhruva, K. Sreenivasan, and V. Cassella, *Phys. Fluids* **12**, 1529 (2000).
 - [5] J. Marshall and F. Schott, *Rev. Geophys.* **37**, 1 (1999).
 - [6] P. Roberts and G. Glatzmaier, *Rev. Mod. Phys.* **72**, 1081 (2000).
 - [7] D. Funfschilling and G. Ahlers, *Phys. Rev. Lett.* **92**, 194502 (2004).
 - [8] E. Brown and G. Ahlers, *J. Fluid Mech.* **568**, 351 (2006).
 - [9] H.-D. Xi, S.-Q. Zhou, Q. Zhou, T.-S. Chan, and K.-Q. Xia, *Phys. Rev. Lett.* **102**, 044503 (2009).
 - [10] J.-Q. Zhong and G. Ahlers, *J. Fluid Mech.* **665**, 300 (2010).

- [11] S. Weiss and G. Ahlers, *J. Fluid Mech.* **688**, 461 (2011).
- [12] K. Sugiyama, R. Ni, R. J. A. M. Stevens, T. S. Chan, S. Q. Zhou, H.-D. Xi, C. Sun, S. Grossmann, K.-Q. Xia, and D. Lohse, *Phys. Rev. Lett.* **105**, 34503 (2010).
- [13] E. Brown and G. Ahlers, *Phys. Rev. Lett.* **98**, 134501 (2007).
- [14] E. Brown and G. Ahlers, *Phys. Fluids* **20**, 075101 (2008).
- [15] M. Assaf, L. Angheluta, and N. Goldenfeld, *Phys. Rev. Lett.* **107**, 044502 (2011).
- [16] Y. Liu and R. E. Ecke, *Phys. Rev. Lett.* **79**, 2257 (1997).
- [17] J. Q. Zhong, R. J. A. M. Stevens, H. J. H. Clercx, R. Verzicco, D. Lohse, and G. Ahlers, *Phys. Rev. Lett.* **102**, 044502 (2009).
- [18] S. Weiss, R. J. A. M. Stevens, J. Q. Zhong, H. J. H. Clercx, D. Lohse, and G. Ahlers, *Phys. Rev. Lett.* **105**, 224501 (2010).
- [19] S. Weiss and G. Ahlers, *J. Fluid Mech.* **684**, 407 (2011).
- [20] R. Stevens, H. Clercx, and D. Lohse, *Phys. Fluids* **22**, 085103 (2010).
- [21] R. J. A. M. Stevens, J. Q. Zhong, H. J. H. Clercx, G. Ahlers, and D. Lohse, *Phys. Rev. Lett.* **103**, 024503 (2009).
- [22] E. Brown and G. Ahlers, *Phys. Fluids* **18**, 125108 (2006).
- [23] F. Zhong, R. Ecke, and V. Steinberg, *J. Fluid Mech.* **249**, 135 (1993).
- [24] P. Vorobieff and R. Ecke, *J. Fluid Mech.* **458**, 191 (2002).